PROCEEDINGS A

royalsocietypublishing.org/journal/rspa

Research

Cite this article: Falkena SKJ, Quinn C, Sieber J, Dijkstra HA. 2021 A delay equation model for the Atlantic Multidecadal Oscillation. *Proc. R. Soc. A* **477**: 20200659.
https://doi.org/10.1098/rspa.2020.0659

Received: 17 August 2020
Accepted: 18 January 2021

Subject Areas:
oceanography, applied mathematics, differential equations

Keywords:
Atlantic Multidecadal Oscillation, Mori–Zwanzig, delay model, reduction methods, conceptual models

Author for correspondence:
Swinda K. J. Falkena
e-mail: s.k.j.falkena@pgr.reading.ac.uk

Electronic supplementary material is available online at https://doi.org/10.6084/m9.figshare.c.5300911.

THE ROYAL SOCIETY PUBLISHING

A delay equation model for the Atlantic Multidecadal Oscillation

Swinda K. J. Falkena[1,2], Courtney Quinn[4,5], Jan Sieber[5] and Henk A. Dijkstra[2,3]

[1]Department of Mathematics and Statistics, University of Reading, Reading, UK
[2]Institute for Marine and Atmospheric Research Utrecht, Department of Physics, and [3]Centre for Complex Systems Studies, Faculty of Science, Utrecht University, Utrecht, The Netherlands
[4]CSIRO Oceans and Atmosphere, Hobart, Tasmania, Australia
[5]Department of Mathematics, University of Exeter, Exeter, UK

SKJF, 0000-0002-2317-9213; JS, 0000-0002-9558-1324

A new technique to derive delay models from systems of partial differential equations, based on the Mori–Zwanzig (MZ) formalism, is used to derive a delay-difference equation model for the Atlantic Multidecadal Oscillation (AMO). The MZ formalism gives a rewriting of the original system of equations, which contains a memory term. This memory term can be related to a delay term in a resulting delay equation. Here, the technique is applied to an idealized, but spatially extended, model of the AMO. The resulting delay-difference model is of a different type than the delay differential model which has been used to describe the El Niño Southern Oscillation. In addition to this model, which can also be obtained by integration along characteristics, error terms for a smoothing approximation of the model have been derived from the MZ formalism. Our new method of deriving delay models from spatially extended models has a large potential to use delay models to study a range of climate variability phenomena.

1. Introduction

To better understand climate variability and climate change often conceptual climate models are used. These models capture the dominant physical processes behind

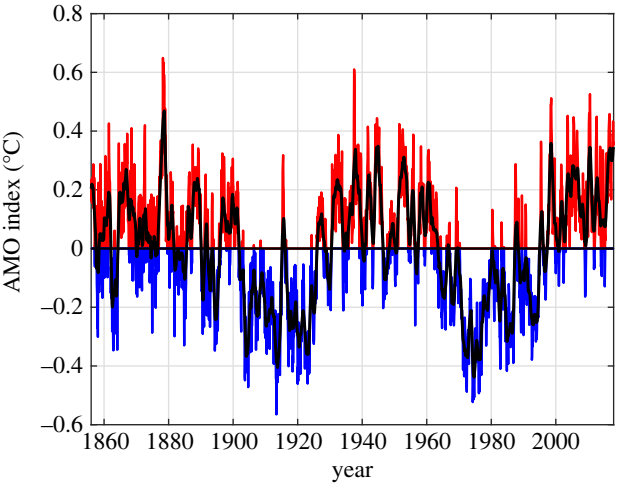

Figure 1. The AMO index for the last 160 years. The index is computed as the deviation of the area-weighted average SST over the North Atlantic. In black, the 12-monthly running mean is shown. Index computed by Enfield *et al.* [5] using the Kaplan SST dataset provided by the NOAA/OAR/ESRL PSD, Boulder, CO, USA (https://www.esrl.noaa.gov/psd/).

climate phenomena, allowing for an improved understanding. Delay equation models form one class of conceptual climate models. These type of models are infinite dimensional, but often depend on only a few variables and parameters. This means that they can potentially describe more complex behaviour than ordinary differential equation (ODE) models, while still being easier to study than multi-dimensional partial differential equation (PDE) models.

Delay models have already been used to describe certain climate phenomena, particularly for the El Niño Southern Oscillation (ENSO) and Earth's energy balance [1]. A new method of deriving delay equation models has been proposed [2], allowing for a potential extension of the use of delay models to study other climate phenomena. This method of deriving delay models is based on the Mori–Zwanzig (MZ) formalism, which allows for the reduction of high-dimensional systems to reduced-order models [3]. These reduced-order models are simpler to study, while still describing the physical processes present in the original high-dimensional model. So far the method in [2] has only been applied to a PDE model of ENSO, for which *ad hoc* delay models were already proposed [4]. Here, we apply the MZ formalism to a PDE model of the Atlantic Multidecadal Oscillation (AMO) to investigate whether this phenomenon can be described by a delay model as well.

The AMO is a pattern of variability in the North Atlantic sea-surface temperature (SST) with a dominant period of 50–70 years [5]. In figure 1 an index for the average SST deviations in the North Atlantic Ocean is shown over the last 160 years. Although the instrumental record is somewhat limited for identifying the dominant time scale and spatial pattern [6], such variability has been detected in proxy data [7] and in global climate models [8–11]. In most theories of the AMO [12] variations in the Atlantic Ocean circulation play a major role. The relevant component of this circulation is the Atlantic Meridional Overturning Circulation (AMOC) [13,14], which is basically the zonally averaged volume transport. The Gulf Stream is part of the AMOC, transporting warm water northwards (and eastwards) which loses heat on its way. At high northern latitudes, the relatively heavy water sinks and flows southwards at larger depths.

One of the proposed physical mechanisms for the AMO, as described in §3, is based on the propagation of so-called thermal Rossby waves [15,16]. The role of these waves in the AMO motivates us to investigate whether its dynamics can be described by a delay model, since the propagation of waves underlies the delay in the ENSO model studied in [2]. Here, we thus apply the MZ formalism to a PDE model of the AMO, using a procedure inspired by [2], with the aim

of deriving a delay model describing the same AMO dynamics. The MZ formalism is general, can be applied to all types of equations (including nonlinear and non-hyperbolic systems) and provides a more formal justification for the use of a conceptual delay model in analysing climate phenomena. This means the method discussed can be applied to other models in which there is a physical mechanism that could cause delayed effects.

The aim of the following study is twofold: to derive a conceptual model with delay for the AMO and to demonstrate the utility and accuracy of doing this with the MZ formalism. We start with a brief description of the MZ formalism in §2, tailored to the problem at hand. Section 3 presents the PDE model of the AMO by Sévellec & Huck [17], which is the starting point for our study. The application of the MZ formalism to this model is discussed in §4, where the resulting model with delay is introduced, as well as a model with delay that can be obtained for the simple PDE system using the method of characteristics (MoC). This leads to a comparison of the delay models and a discussion of the errors introduced by using the MZ formalism in §5. A summary and discussion follows in §6.

2. Mori–Zwanzig formalism

The MZ formalism provides a way of reducing a high-dimensional model to a reduced-order, more tractable system. The formalism is based on the work by Mori [18] and Zwanzig [19] in statistical mechanics. It has been reformulated to be suitable for constructing reduced-order models for systems of ODEs [3,20,21]. When studying applications in climate one often has to deal with PDEs, making the application of the formalism challenging. In this section, we start with a general overview of the MZ formalism based on [3], followed by a more detailed discussion of the particulars of applying the formalism to PDEs.

For a vector of state variables $\phi(x,t) \in \mathbb{R}^n$ which are continuously differentiable in $t \in \mathbb{R}_+$ and initial conditions $x \in \mathbb{R}^n$, we consider the system of ODEs defining the dynamics

$$\frac{\mathrm{d}}{\mathrm{d}t}\phi(x,t) = R(\phi(x,t)), \quad \phi(x,0) = x, \tag{2.1}$$

where $R : \mathbb{R}^n \to \mathbb{R}^n$ is the vector-valued function of the specific system with components R_i. Now consider the evolution of an observable $u(x,t) := g(\phi(x,t))$ along a trajectory $\phi : \mathbb{R}^n \times \mathbb{R}_+ \to \mathbb{R}^n$. This observable satisfies the PDE

$$\frac{\partial}{\partial t}u(x,t) = \mathcal{L}u(x,t), \quad u(x,0) = g(x), \tag{2.2}$$

where $\mathcal{L}$ is the Liouville operator (or generator) [22] given by

$$[\mathcal{L}u](x) = \sum_{i=1}^{n} R_i(x)\partial_{x_i}u(x). \tag{2.3}$$

Note that, for a linear system where R is defined by a matrix A having elements A_{ij}, the Liouville operator reads $[\mathcal{L}u](x) = \sum_{i=1}^{n}\sum_{j=1}^{n} A_{ij}x_j\partial_{x_i}u(x)$.

To arrive at a reduced-order model for the dynamics governing $\phi(x,t)$, one needs to decide on the resolved variables $\hat{\phi} \in \mathbb{R}^m$. In our illustration, we take $\hat{\phi}$ as a subset of m components ϕ_i for some indices i. We also make a choice for an appropriate projection operator $P : C(\mathbb{R}^n, \mathbb{R}^k) \to C(\mathbb{R}^m, \mathbb{R}^k)$ onto these variables. Examples of projection operators are the linear projection, setting all unresolved variables to zero, and the conditional expectation [3]. Let $Q = I - P$ denote the complement of P (with I the identity operator). Furthermore, we use the notation $[PR_i](\phi(x,t)) = R_i([\hat{\phi}(x,t),0]) = R_i(\hat{\phi}(x,t))$. We consider the choice of setting unresolved variables to zero for our projection P, such that, for an arbitrary observable $g \in C(\mathbb{R}^n, \mathbb{R}^k)$ (with arbitrary $k \geq 1$), the projection P is defined as $[Pg](\phi(x,t)) := g([\hat{\phi}(x,t),0])$.

Having chosen a set of resolved variables and a projection operator P, the reduced-order model corresponding to the full system (2.1) is given by the generalized Langevin equation (see Chorin

et al. [3] for its derivation),

$$\frac{\partial}{\partial t}\phi_i(x,t) = R_i([\hat{\phi}(x,t),0]) + F_i(x,t) + \int_0^t K_i([\hat{\phi}(x,t-s),0],s)\mathrm{d}s, \tag{2.4}$$

where $\phi_i(x,t)$ is one of the resolved variables. The functions F_i and K_i are defined as

$$F_i(x,t) = [\mathrm{e}^{tQ\mathcal{L}}Q\mathcal{L}](x) \quad \text{and} \quad K_i(\hat{x},t) = [P\mathcal{L}F_i](\hat{x},t), \tag{2.5}$$

where $\hat{x}$ denotes the resolved part of the initial conditions x. The terms on the right-hand side of the Langevin equation are often referred to as the Markovian term $R_i(\hat{\phi}(x,t))$, the noise term $F_i(x,t)$ and the memory term, being the integral over $K_i(\hat{\phi}(x,t-s),s)$. For a linear system, this memory integrand is obtained by applying a memory kernel to the resolved variables, i.e. $K_i(\hat{\phi}(x,t-s),s) = \hat{K}_i(s)[\hat{\phi}(x,t-s)]$.

The main difficulty in the application of the MZ formalism is calculating the terms F_i, which enter in the noise and the memory terms and which are the solutions of the orthogonal dynamics equation

$$\frac{\partial}{\partial t}F_i(x,t) = Q\mathcal{L}F_i(x,t), \quad F_i(x,0) = Q\mathcal{L}x_i. \tag{2.6}$$

In general, it is not known if the system (2.6) is well posed. However, for specific cases it is possible to find approximate solutions. The possibility and difficulty of finding these solutions strongly depends on the choice of the resolved variables and projection operator. A suitable choice would yield an orthogonal dynamics system which can be solved in a more straightforward manner than the full system. In some cases the choice for the resolved variables and corresponding projection can be motivated by physical arguments for the specific system. For other models the choice might not be as straightforward and one cannot be certain that a suitable reduced-order model exists.

When the ODE system studied is linear, i.e. $R(\phi(x,t)) = A\phi(x,t)$, where A is a constant matrix, finding a suitable set of resolved variables can be done by looking at the eigenvalues of the orthogonal dynamics system. When the system (2.1) is linear, the behaviour of the orthogonal dynamics can be obtained by studying the eigenvalues of $A_Q = A - PA$. A set of resolved variables is suitable if the eigenvalues of the orthogonal dynamics system show significantly more stability, i.e. have more negative real parts than the full system. If this is not the case the problem of solving the full system is transferred to the equally difficult problem of solving the orthogonal dynamics system.

Up until now, we have not discussed the difficulties arising when the MZ formalism is applied to a PDE system instead of ODEs. When the system is Hamiltonian some results exist (e.g. [20]); however, when this is not the case often the system is expanded in a basis of typically orthonormal functions (e.g. [21,23]) to numerically find a solution. If the aim of applying the MZ formalism is to obtain a set of reduced-order model equations and not only a numerical result, this method is not suitable. Another approach, relying on integration along characteristics, has been explored by Falkena *et al.* [2] and yielded an exact reduced-order (delay) model for the system studied. Here, we build on this work to see whether delay-type models can be derived for other systems of wave equations. In particular, we focus on a PDE model that describes thermal Rossby wave propagation related to the AMO. This model is introduced in the next section.

3. Atlantic Multidecadal Oscillation

The thermal Rossby wave mechanism, suggested to be responsible for the AMO [15,16], is summarized in figure 2. When there is a positive temperature anomaly (T') in the northern-central part of the basin, the meridional temperature gradient becomes stronger with respect to the background state. This results in a zonal overturning anomaly with westward surface flow through thermal wind balance (figure 2*a*). The negative zonal flow transports the positive temperature anomaly towards the western boundary, creating a zonal temperature gradient. Again through thermal wind balance, this now leads to anomalies in the meridional overturning circulation (figure 2*b*). This flow transports cold water from near the poles southwards, reducing

the meridional temperature gradient. This smaller north–south temperature gradient causes a positive (eastward) zonal flow, after which the same pattern as described above is followed with a sign change. Hence, the variability associated with the AMO relies on the transport of heat and the flow response through the thermal wind balance [24].

Low-order *ad hoc* ODE models of the AMO have been studied by, among others, Broer *et al.* [25]. More recently, Sévellec & Huck [17] developed an idealized PDE model of the AMO to which we apply the MZ formalism. This PDE model roughly captures the thermal Rossby wave mechanism described before, but with a simplification of the associated wave dynamics. In this section, we present this model and briefly discuss its derivation. In addition, we investigate the effect of using a more realistic strictly positive meridional overturning circulation as the background state on the behaviour of the model introduced in [17].

(a) Model formulation

The AMO model by Sévellec & Huck [17] is a three-layer model describing the evolution of temperature perturbations in the North Atlantic Ocean. The model describes the temperatures (T_i, $i=1,2,3$) as a function of longitude (x) and time (t). For convenience, we consider the non-dimensional version of the model with longitude-scale W (basin width) and time scale Y (a year).

The scaled model is

$$\left.\begin{aligned}\partial_t T_1 &= a_1\partial_x T_1 + b_1\partial_x T_2 + c_1\partial_x T_3 + \kappa_s\partial_{xx}T_1,\\ \partial_t T_2 &= a_2\partial_x T_1 + b_2\partial_x T_2 + c_2\partial_x T_3 + \kappa_s\partial_{xx}T_2\end{aligned}\right\} \tag{3.1}$$

and

$$\partial_t T_3 = \kappa_s\partial_{xx}T_3,$$

with boundary conditions

$$T_i(x|_{\text{West}}=0) = -T_i(x|_{\text{East}}=1), \quad i=1,2,3. \tag{3.2}$$

The constants in the model are all positive for physically realistic values and are defined by

$$\left.\begin{aligned}a_1 &= \frac{Y}{W}\left(\frac{\alpha_T g}{2Hf}\left(-h_1(h_2+h_3)\partial_y\bar{T} + \frac{\beta}{2f}h_1^2(h_2+h_3)\partial_z\bar{T}\right) - \bar{u}\right),\\ b_1 &= \frac{Y}{W}\frac{\alpha_T g}{2Hf}\left(-h_2(h_2+2h_3)\partial_y\bar{T} + \frac{\beta}{2f}h_1h_2(h_2+2h_3)\partial_z\bar{T}\right),\\ c_1 &= \frac{Y}{W}\frac{\alpha_T g}{2Hf}\left(-h_3^2\partial_y\bar{T} + \frac{\beta}{2f}h_1h_3^2\partial_z\bar{T}\right),\\ a_2 &= \frac{Y}{W}\frac{\alpha_T g}{2Hf}\left(h_1^2\partial_y\bar{T} + \frac{\beta}{2f}h_1^2(h_2+2h_3)\partial_z\bar{T}\right),\\ b_2 &= \frac{Y}{W}\left(\frac{\alpha_T g}{2Hf}\left(-h_2(h_3-h_1)\partial_y\bar{T} + \frac{\beta}{2f}(4h_1h_2h_3 + h_2^2(h_1+h_3))\partial_z\bar{T}\right) - \bar{u}\right),\\ c_2 &= \frac{Y}{W}\frac{\alpha_T g}{2Hf}\left(-h_3^2\partial_y\bar{T} + \frac{\beta}{2f}h_3^2(2h_1+h_2)\partial_z\bar{T}\right)\end{aligned}\right\} \tag{3.3}$$

and

$$\kappa_s = \kappa\frac{Y}{W^2}.$$

The values of the parameters needed to compute these constants are given in table 1.

The derivation of these equations can be found in [17]. Here, we briefly discuss that derivation and assumptions made to get to the above system of equations (3.1). The derivation starts from an advection–diffusion equation for temperature, geostrophic balance (a balance between the horizontal pressure gradients and the Coriolis force), hydrostatic balance (a balance between the vertical pressure gradient and gravity) and a linear dependence of density on temperature. The equations for temperature are linearized around a fixed background state comprising zonal flow $\bar{u}$ and temperature gradients in the meridional $\partial_y\bar{T}$ and vertical $\partial_z\bar{T}$ (figure 3). Note that this

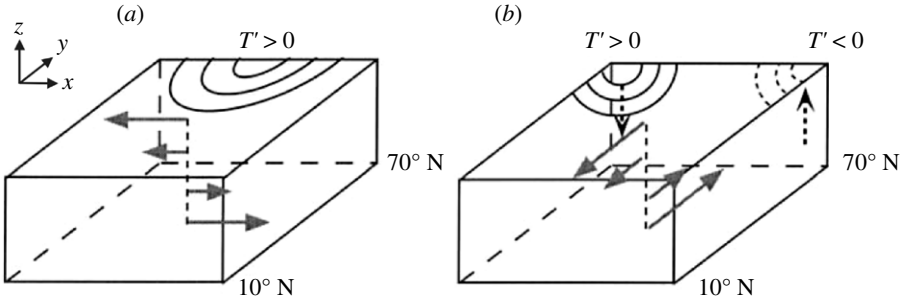

Figure 2. Schematic diagram of the physical mechanism responsible for the AMO with two phases a quarter period apart in (*a*) and (*b*). Figure taken from [24].

Table 1. The values of the parameters in the AMO model by Sévellec & Huck [17].

thickness layer 1	h_1	600 m	
thickness layer 2	h_2	600 m	vertical temperature gradient
thickness layer 3	h_3	3300 m	
total ocean depth	H	4500 m	$\partial_z \bar{T} = -\frac{2C}{h_1+h_2}(\Delta T - \frac{\alpha_S}{\alpha_T}\Delta S)$
zonal basin size	W	4000 km	
meridional basin size	L	6500 km	control parameter C
time scale (year)	Y	3.1536×10^7 s	standard $C = 1$
horizontal diffusivity	κ	2×10^3 m^2 s^{-1}	
acceleration of gravity	g	9.8 m s^{-2}	
Coriolis parameter	f	10^{-4} s^{-1}	
β effect	β	1.5×10^{-11} (ms)$^{-1}$	meridional temperature gradient
thermal expansion coefficient	α_T	2×10^{-4} K^{-1}	
haline contraction coefficient	α_S	7×10^{-4} psu^{-1}	$\partial_y \bar{T} = \frac{2}{L}(\Delta T - \frac{\alpha_S}{\alpha_T}\Delta S)$
meridional temperature difference	ΔT	−20 K	
meridional salinity difference	ΔS	−1.5 psu	
zonal velocity	$\bar{u}$	10^{-2} m s^{-1}	

means that the overturning circulation ($\bar{v}$, $\bar{w}$) is neglected because of its weakness with respect to the zonal flow. The linearized temperature equation is then discretized over three layers assuming no flow through the surface and bottom and no background flow or temperature gradients in the bottom layer, which results in system (3.1).

As the model assumes geostrophic balance, (3.1) only describes the solution of the interior part of the basin. The boundary conditions (3.2) are therefore derived by considering an additional boundary layer at either end of the basin with free-slip conditions at the interface between the interior flow and the boundary, and zero heat flux assumptions at the outer edges of the boundary layer (ocean basin walls). The full derivation can be found in the appendix of [17]. Since the boundary conditions at hand will prove essential for our results, we explain the physics behind the coupling between the two boundaries. A signal, in the form of a Rossby wave, arriving at the western boundary of the basin, travels south, along the equator and back up north in the form of a Kelvin wave. Since the time scale of Kelvin waves is much shorter than that of the Rossby waves present in the model, this adjustment is assumed to be instantaneous. This leads to the coupling of the two boundaries and allows for waves to keep propagating through the basin. For the specifics on the change of sign we refer the reader to the derivation of the boundary conditions in [17].

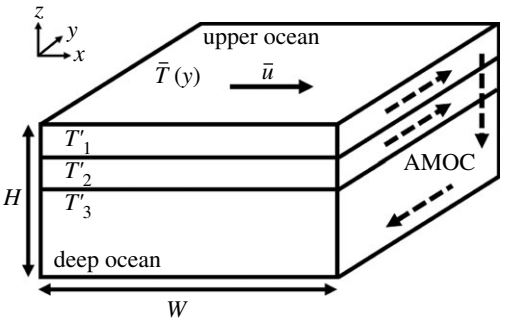

Figure 3. A schematic diagram of the three-layer ocean basin considered in the AMO model. The dashed arrows show the background AMOC, which is taken into account in the background state of the model discussed in §3b.

Table 2. The numerical values of the parameters in equation (3.4). We note that α is a free parameter of $\mathcal{O}(10^{-3})$ and throughout this article we will use $\alpha = 0$ to explore the undamped solutions of equation (3.4).

a_1	a_2	b_1	b_2
0.1479	0.0540	0.4187	0.2423

Using, for example, a no-flux boundary is not valid here, as it would assume geostrophic balance in the boundary layer and neglect these Kelvin waves, making the model no longer dynamically accurate or suitable to study the AMO dynamics.

In this paper two additional simplifications to the model (3.1) are made. Firstly, we note that the only term acting in the third layer is diffusion and the two top layers do not couple into it. As a result any perturbation in that layer eventually damps out. For this reason, and to simplify the mathematical treatment of the system, perturbations in the bottom layer are neglected (i.e. $T_3 = 0$). Secondly, we approximate the diffusion terms by linear damping with damping coefficient α. The system (3.1) then simplifies to a two-layer system,

$$\left.\begin{aligned} \partial_t T_1 &= a_1 \partial_x T_1 + b_1 \partial_x T_2 - \alpha T_1 \\ \text{and} \qquad \partial_t T_2 &= a_2 \partial_x T_1 + b_2 \partial_x T_2 - \alpha T_2. \end{aligned}\right\} \tag{3.4}$$

This is the AMO model to which we apply the MZ formalism. Also note that this temperature model explains changes in the overturning circulation as well, via thermal wind balance, the continuity equation and Sverdrup balance, which is discussed in the electronic supplementary material. The parameter values used for the numerical results in the remainder of this section and the coming sections are given in table 2.

Before looking into the application of the MZ formalism to this AMO model, we illustrate its behaviour by simulating it for $\alpha = 0$. We use an upwind discretization scheme for the x-derivatives and a forward Euler scheme in time. Note that this discretization introduces numerical diffusion, leading to artificial damping effects. The result is shown in figure 4. Note the opposite sign of the temperature in the two layers, which is due to the baroclinic nature of the waves [26]. The model shows a combination of two oscillations with different periods. Firstly, there is a long period of approximately 60 years, which corresponds to a thermal Rossby wave responsible for driving the AMO. Secondly, there is a higher frequency oscillation with a period of around 5 years.

The occurrence of the shorter period is at first sight surprising as it is not found in more detailed PDE models. This oscillation does not correspond to a planetary Rossby wave, as one might expect, since decreasing β does not result in a disappearance of these oscillations. It is a thermal Rossby wave, just as the one responsible for the oscillation associated with the AMO. The dominant appearance of this thermal Rossby wave in the model is undesired when studying

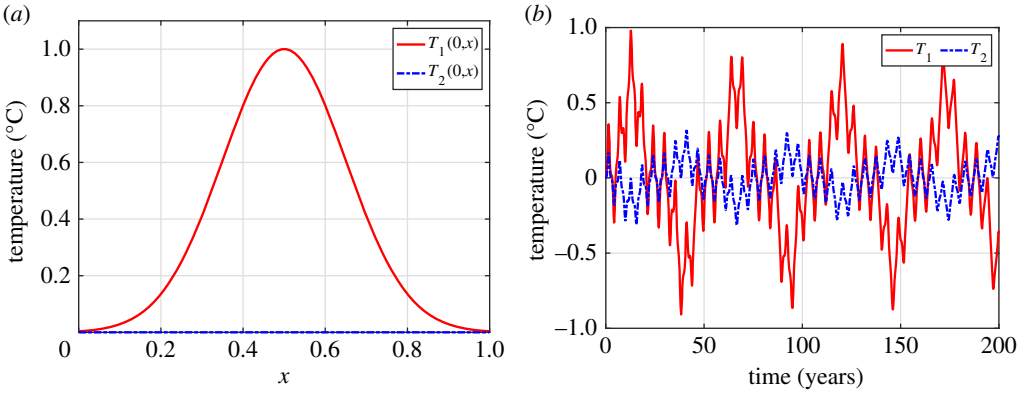

Figure 4. Model simulation of the temperature anomaly in the AMO model (equation (3.4)) for an initial positive Gaussian temperature perturbation in the centre of the basin in the first layer ($\Delta t = \Delta x = 0.0005, \alpha = 0$). (*a*) The initial conditions. (*b*) Evolution of model (3.4) at $x = 0$. (Online version in colour.)

the AMO. A possible improvement of the model, resulting in the damping of this high-frequency mode, is discussed in the next section.

(b) Background overturning circulation

The AMO model by Sévellec & Huck [17] described in the previous section does not contain an overturning circulation in the background state, as the background meridional ($\bar{v}$) and vertical ($\bar{w}$) velocities are neglected. This means that in the model the overturning circulation, which can be inferred from the temperature evolution (details are given in the electronic supplementary material), can become negative. To prevent this from happening in the model, we consider an extended background state which retains meridional $\bar{v}$ and vertical $\bar{w}$ flow (figure 3, dashed arrows). With this different background state an extended two-layer temperature model for AMO can be derived following the same steps as in [17]. The details of this derivation can be found in the electronic supplementary material. The resulting system for temperature in the two upper layers is

$$\left.\begin{aligned} \partial_t T_1 &= a_1 \partial_x T_1 + b_1 \partial_x T_2 - (\beta_1 + \alpha) T_1 - \beta_2 T_2 \\ \text{and} \quad \partial_t T_2 &= a_2 \partial_x T_1 + b_2 \partial_x T_2 - (\beta_3 + \alpha) T_2, \end{aligned}\right\} \tag{3.5}$$

where

$$\beta_1 = Y \cdot \left(\frac{\beta}{f}\bar{v} + \frac{2}{h_1}\bar{w}\right), \quad \beta_2 = -Y\frac{4}{h_1}\bar{w} \quad \text{and} \quad \beta_3 = Y \cdot \left(\frac{\beta}{f}\bar{v} + \frac{2}{h_2}\bar{w}\right). \tag{3.6}$$

The difference from (3.4) is that there are additional linear terms in both equations. Note that not all the additional terms have a damping effect, as some of the β_i-terms can be negative.

A model simulation for $\bar{v} = 0.5 \times 10^{-2}\,\mathrm{m\,s^{-1}}$ and $\bar{w} = -0.17 \times 10^{-6}\,\mathrm{m\,s^{-1}}$ is shown in figure 5, where the values are chosen for plotting purposes within a realistic range. Note that, if $-2\bar{w}/h_{1,2} \gg \beta\bar{v}/f$, we have that $\beta_{1,3}$ become strongly negative, leading to possible unstable solutions or at least amplifying effects within the solution. The result of adding the background overturning circulation is a damping of the high-frequency oscillation, as can be seen in figure 5. This short period oscillation is absorbed by the background overturning circulation while the long period oscillation persists. The amplitude of the oscillation corresponding to the AMO is not noticeably affected by the damping. This can be due to the presence of an amplifying effect of the background overturning in some parts of the equations, as mentioned previously. For simplicity, we apply the MZ formalism to the AMO model as given in equation (3.4) instead of the extended model discussed here. The application of the MZ formalism to this extended

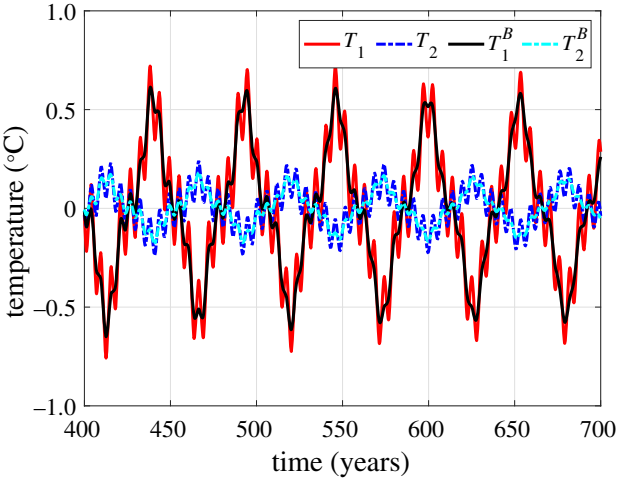

Figure 5. Simulations of the temperature in the two layers without (solid red T_1, dashed blue T_2) and with (solid black T_1^B, dashed cyan T_2^B) a background overturning circulation ($\beta_1 = \beta_3 = 1.156 \times 10^{-3}$, $\beta_2 = 7.148 \times 10^{-3}$, $\alpha = 0$). (Online version in colour.)

model can be found in the electronic supplementary material. This derivation follows the exact same steps as discussed in the following sections. We note that the results are similar to those discussed in the following, but for the extended model additional factors that lead to the decay of the high-frequency mode emerge. This is discussed in more detail at the end of §4c.

4. Reduction to a delay model

The aim of applying the MZ formalism to the AMO model described in §3 is to arrive at a projected model describing the same dynamics as the full model and analyse the effect of memory in that system, with the potential of deriving a delay model for the phenomenon. A similar procedure has been applied to a model of the ENSO by Falkena *et al.* [2]. A difference is that for the AMO no previously proposed delay model is known. Therefore, it is not immediately clear how to choose a projection, nor how to deal with solving the subsequent orthogonal dynamics equation (2.6). Preferably, we arrive at an equation for the temperature at one location in space, to remove the explicit dependency on x in the system, but it is not clear from the outset whether or not this is feasible.

The way in which we proceed is to first convert the system of PDEs (3.4) into a set of ODEs by discretization. To this high-dimensional system of ODEs, the MZ formalism is then applied. This procedure is described in the following sections. After deciding on the discretization to use, possible (sets of) resolved variables are explored, followed by a discussion of the different terms in the Langevin equation (2.4).

(a) Discretization

The first step is to find a stable discretization of the AMO model in equation (3.4). A grid of $(N+1)$-points in space with distance $dx = \frac{1}{N}$ is used. Because all parameters in the model are positive we know that all waves travel westwards. Therefore, we use an upwind scheme to discretize the model. The discretized equations are

$$\left.\begin{aligned} \partial_t T_1^n &= \frac{a_1}{\mathrm{d}x}(T_1^{n+1} - T_1^n) + \frac{b_1}{\mathrm{d}x}(T_2^{n+1} - T_2^n) - \alpha T_1^n \\ \text{and} \quad \partial_t T_2^n &= \frac{a_2}{\mathrm{d}x}(T_1^{n+1} - T_1^n) + \frac{b_2}{\mathrm{d}x}(T_2^{n+1} - T_2^n) - \alpha T_2^n, \end{aligned}\right\} \tag{4.1}$$

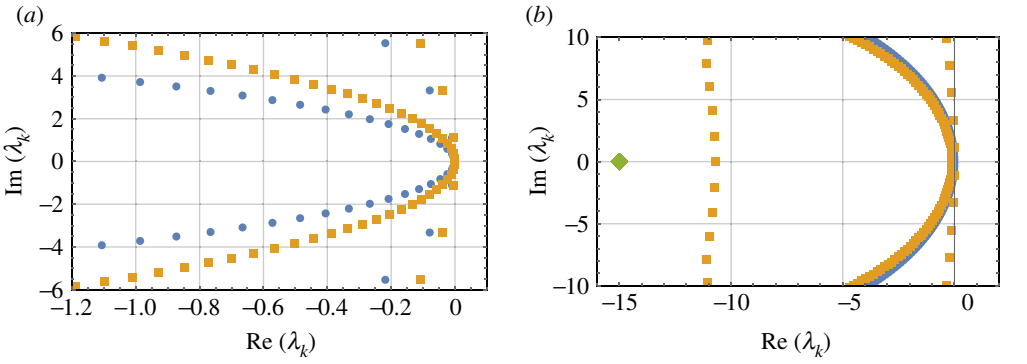

Figure 6. The eigenvalues of the discretized AMO model ($\alpha = 0.001$) (*a*) for different N and (*b*) different sets of resolved variables. Note that not all eigenvalues are shown (e.g. only one of the two eigenvalues for the projection onto T_1^0 and T_2^0, the second one is more negative). (*a*) Full model for $N = 200$ (blue, circles) and $N = 400$ (yellow, squares). (*b*) Full model for $N = 400$ (blue, circles) and using a projection onto either T_1^0 (yellow, squares) or both T_1^0 and T_2^0 (green, diamond). (Online version in colour.)

for $n = 0, \ldots, N$ (such that $T_i^k \approx T_i(k/N)$), with boundary conditions

$$T_1^N = -T_1^0, \quad T_2^N = -T_2^0. \tag{4.2}$$

By the circular nature of the boundary conditions this is a $2N$-dimensional system (there is no need to solve the dynamical equations for discretization points N). Letting $N \to \infty$ recovers the PDE model exactly. This system (4.1) can be written as a matrix equation for $\vec{T} = (T_1^0, T_2^0, \ldots, T_1^{N-1}, T_2^{N-1})$,

$$\partial_t \vec{T} = M\vec{T}. \tag{4.3}$$

The construction of M is straightforward from system (4.1).

The stability of the solution of this discretized system of ODEs is verified by computing the eigenvalues of the matrix M. These are shown in figure 6*a* for $N = 200$ (blue circles) and $N = 400$ (yellow squares). For each N two sets of eigenvalues are visible, with the spacing between the imaginary part of the eigenvalues in either set equal to the corresponding wave frequency. For increasing N both curves of eigenvalues approach a line with real part $-\alpha$, where the eigenvalues of the continuous system are. Since all eigenvalues are negative for every N the discretization is stable. In the following sections, we go into the application of the MZ formalism to this system of ODEs.

(b) Projection

When applying the MZ formalism the first step is to choose the resolved variables and corresponding projection. As discussed in §2, this is an essential choice determining the final expressions in the Langevin equation (2.4). From the modelling perspective, the aim is to find a system of equations for the temperature at one location in order to remove the x-dependency of the system. With this in mind there are three possible choices for the resolved variables: T_1, T_2, and both. Note that because all waves travel in the same direction without loss of energy it does not matter on which location in space the temperatures are projected. For convenience, we choose to project onto the western boundary ($n = 0$), but note that the result for any other location is the same. The most straightforward way to project onto one of those sets of resolved variables is to use the linear projection P that sets all unresolved variables to zero. Its complement Q thus sets the resolved variables to zero since the system considered is linear. The corresponding orthogonal

dynamics equation (2.6) can be written as a matrix equation

$$\partial_t \vec{T}_Q = M_Q \vec{T}_Q, \tag{4.4}$$

where $\vec{T}_Q = (T^1_{1Q}, T^1_{2Q}, \ldots, T^{N-1}_{1Q}, T^{N-1}_{2Q})$ represents the unresolved variables. The matrix M_Q is the same as the matrix for the full system M, but with the rows and columns corresponding to the resolved variable(s) removed.

To assess the quality of the three possible projections, we study the eigenvalues of the corresponding orthogonal dynamics systems. A sufficient decay of the eigenvalues of the orthogonal dynamics system indicates that the corresponding resolved variables and projections are suitable as discussed in §2. In figure 6*b*, the eigenvalues of the full system and projected systems are shown for two different projections on boundary variables. When one projects onto only T^0_1 the eigenvalues are quite similar to those of the original system. Similar results are found for projection onto only T^0_2.

If both T^0_1 and T^0_2 are taken as the resolved variables the result is noticeably better. The orthogonal dynamics system has only two eigenvalues, which become increasingly negative with increasing N. Therefore, this projection onto both T_1 and T_2 at the boundary $x = 0$ is chosen, where we note once again that the choice of the specific location is arbitrary. In the following section we focus on the derivation of the noise and memory term in the MZ formalism (2.5). Here, we briefly discuss the Markovian terms. They are given by the projection of the right-hand side of the equations for T^0_1 and T^0_2 (equation (4.1) for $n = 0$),

$$\left.\begin{aligned} P\left[\frac{a_1}{\mathrm{d}x}(T^1_1 - T^0_1) + \frac{b_1}{\mathrm{d}x}(T^1_2 - T^0_2) - \alpha T^0_1\right] &= -\frac{a_1}{\mathrm{d}x}T^0_1 - \frac{b_1}{\mathrm{d}x}T^0_2 - \alpha T^0_1 \\ \text{and} \qquad P\left[\frac{a_2}{\mathrm{d}x}(T^1_1 - T^0_1) + \frac{b_2}{\mathrm{d}x}(T^1_2 - T^0_2) - \alpha T^0_2\right] &= -\frac{a_2}{\mathrm{d}x}T^0_1 - \frac{b_2}{\mathrm{d}x}T^0_2 - \alpha T^0_2. \end{aligned}\right\} \tag{4.5}$$

This simply is the right-hand side dependence of equation (4.1) on the resolved variables, as a linear projection is used.

(c) Noise and memory terms

To compute the noise and memory term, we focus on the orthogonal dynamics system (4.4). For the chosen resolved variables T^0_1 and T^0_2 with the linear projection the matrix reads

$$M_Q = \begin{pmatrix} -\frac{a_1}{\mathrm{d}x} - \alpha & -\frac{b_1}{\mathrm{d}x} & \frac{a_1}{\mathrm{d}x} & \frac{b_1}{\mathrm{d}x} & & & & \\ -\frac{a_2}{\mathrm{d}x} & -\frac{b_2}{\mathrm{d}x} - \alpha & \frac{a_2}{\mathrm{d}x} & \frac{b_2}{\mathrm{d}x} & & & & \\ & & -\frac{a_1}{\mathrm{d}x} - \alpha & -\frac{b_1}{\mathrm{d}x} & \ddots & & & \\ & & -\frac{a_2}{\mathrm{d}x} & -\frac{b_2}{\mathrm{d}x} - \alpha & \ddots & & & \\ & & & & \ddots & \frac{a_1}{\mathrm{d}x} & \frac{b_1}{\mathrm{d}x} & \\ & & & & \ddots & \frac{a_2}{\mathrm{d}x} & \frac{b_2}{\mathrm{d}x} & \\ & & & & & -\frac{a_1}{\mathrm{d}x} - \alpha & -\frac{b_1}{\mathrm{d}x} & \\ & & & & & -\frac{a_2}{\mathrm{d}x} & -\frac{b_2}{\mathrm{d}x} - \alpha \end{pmatrix}. \tag{4.6}$$

Note that this matrix is block upper diagonal with all blocks on the diagonal being the same. To solve the orthogonal dynamics system, we have to find the eigenvalues and (generalized)

eigenvectors of this matrix M_Q. As discussed in §4b, there are only two eigenvalues

$$\lambda_\pm = -\alpha - \frac{l_\pm}{\mathrm{d}x}, \tag{4.7}$$

with

$$l_\pm = \frac{1}{2}\left(a_1 + b_2 \pm \sqrt{a_1^2 + b_2^2 - 2a_1b_2 + 4a_2b_1}\right), \tag{4.8}$$

each of multiplicity $N-1$. Note that $l_\pm$ yield the characteristics of the original PDE system (3.4). The corresponding generalized eigenvectors for $i = 1, \ldots, N-1$ are

$$\vec{v}_\pm^{\,i} = \left(\frac{\mathrm{d}x}{l_\pm}\right)^{i-1} \cdot (0, \ldots, 0, w_\pm, 1, 0, \ldots, 0), \tag{4.9}$$

where the non-zero values are located on the coordinates corresponding to location i. Here,

$$w_\pm = \frac{1}{2a_2}\left(a_1 - b_2 \pm \sqrt{a_1^2 + b_2^2 - 2a_1b_2 + 4a_2b_1}\right). \tag{4.10}$$

Having computed the eigenvalues and eigenvectors we can write down the solutions $\vec{T}_Q$ of the orthogonal dynamics equation (e.g. [27]). Here, we only note that $\vec{T}_Q$ is a linear combination of the eigenvectors, meaning it is relatively straightforward to identify the solution at one location. The full expressions are given in the electronic supplementary material, together with the use of initial conditions to determine the constants involved.

Now that we have the solution to the orthogonal dynamics equation we can write down the noise terms and subsequently compute the memory terms of the discretized AMO system (4.1). The noise terms are defined by

$$\left.\begin{aligned} F_{T_1^0}(t) &= \frac{a_1}{\mathrm{d}x}T_{1Q}^1(t) + \frac{b_1}{\mathrm{d}x}T_{2Q}^1(t) \\ \text{and} \qquad F_{T_2^0}(t) &= \frac{a_2}{\mathrm{d}x}T_{1Q}^1(t) + \frac{b_2}{\mathrm{d}x}T_{2Q}^1(t). \end{aligned}\right\} \tag{4.11}$$

Note that only the terms of the solution $\vec{T}_Q$ which contain the eigenvectors $\vec{v}_\pm^{\,1}$ contribute to the noise term, as all other eigenvectors have zeros in the direction of T_{1Q}^1 and T_{2Q}^1. The resulting expressions, following the solution of equation (4.4), are

$$\left.\begin{aligned} F_{T_1^0}(t) &= N\sum_{i=1}^{N-1}\left((a_1w_+ + b_1)\,\mathrm{e}^{\lambda_+ t}c_+^i + (a_1w_- + b_1)\,\mathrm{e}^{\lambda_- t}c_-^i\right)\frac{t^{i-1}}{(i-1)!} \\ \text{and} \qquad F_{T_2^0}(t) &= N\sum_{i=1}^{N-1}\left((a_2w_+ + b_2)\,\mathrm{e}^{\lambda_+ t}c_+^i + (a_2w_- + b_2)\,\mathrm{e}^{\lambda_- t}c_-^i\right)\frac{t^{i-1}}{(i-1)!}, \end{aligned}\right\} \tag{4.12}$$

where

$$\left.\begin{aligned} c_+^i &= \left(\frac{l_+}{\mathrm{d}x}\right)^{i-1} \cdot \frac{T_1^i(0) - w_-T_2^i(0)}{w_+ - w_-} \\ \text{and} \qquad c_-^i &= -\left(\frac{l_-}{\mathrm{d}x}\right)^{i-1} \cdot \frac{T_1^i(0) - w_+T_2^i(0)}{w_+ - w_-} \end{aligned}\right\} \tag{4.13}$$

depend on the initial conditions of the unresolved variables.

To compute the memory terms (as defined in (2.5)), we first look at the effect of applying the operator $P\mathcal{L}$ to each of the initial conditions. This is sufficient for computation of the memory

terms because the noise terms (4.12) are linear in the initial conditions. We find

$$\begin{aligned}
&P\mathcal{L}\big(T_1^1(0), T_2^1(0), \ldots, T_1^i(0), T_2^i(0), \ldots, T_1^{N-1}(0), T_2^{N-1}(0)\big)\\
&\quad = P\bigg(\cdots, \frac{a_1}{\mathrm{d}x}(T_1^{i+1}(0) - T_1^i(0)) + \frac{b_1}{\mathrm{d}x}(T_2^{i+1}(0) - T_2^i(0)) - \alpha T_1^i(0),\\
&\qquad \frac{a_2}{\mathrm{d}x}(T_1^{i+1}(0) - T_1^i(0)) + \frac{b_2}{\mathrm{d}x}(T_2^{i+1}(0) - T_2^i(0)) - \alpha T_2^i(0), \ldots \bigg)\\
&\quad = \bigg(0, \ldots, 0, -\frac{a_1}{\mathrm{d}x}T_1^0(0) - \frac{b_1}{\mathrm{d}x}T_2^0(0), -\frac{a_2}{\mathrm{d}x}T_1^0(0) - \frac{b_2}{\mathrm{d}x}T_2^0(0)\bigg).
\end{aligned} \tag{4.14}$$

We see that only terms that initially depend on $T_1^{N-1}(0)$ and $T_2^{N-1}(0)$ are non-zero after application of $P\mathcal{L}$. Combining this result with the noise term (4.12) and replacing dx by $\frac{1}{N}$, the memory integrand (2.5) becomes

$$\left.\begin{aligned}
K_{T_1^0}((T_1^0(0), T_2^0(0)), t) &= N^2 \frac{t^{N-2}}{(N-2)!}\,\mathrm{e}^{-\alpha t}\Big((l_+N)^{N-2}\,\mathrm{e}^{-l_+Nt}\big(A_{1+}T_1^0(0) + B_{1+}T_2^0(0)\big)\\
&\quad + (l_-N)^{N-2}\,\mathrm{e}^{-l_-Nt}\big(A_{1-}T_1^0(0) + B_{1-}T_2^0(0)\big)\Big),\\
K_{T_2^0}((T_1^0(0), T_2^0(0)), t) &= N^2 \frac{t^{N-2}}{(N-2)!}\,\mathrm{e}^{-\alpha t}\Big((l_+N)^{N-2}\,\mathrm{e}^{-l_+Nt}\big(A_{2+}T_1^0(0) + B_{2+}T_2^0(0)\big)\\
&\quad + (l_-N)^{N-2}\,\mathrm{e}^{-l_-Nt}\big(A_{2-}T_1^0(0) + B_{2-}T_2^0(0)\big)\Big),
\end{aligned}\right\} \tag{4.15}$$

with

$$\left.\begin{aligned}
A_{1+} &= \frac{(a_1w_+ + b_1)(-a_1 + w_-a_2)}{w_+ - w_-}, \quad A_{1-} = \frac{-(a_1w_- + b_1)(-a_1 + w_+a_2)}{w_+ - w_-},\\
B_{1+} &= \frac{(a_1w_+ + b_1)(-b_1 + w_-b_2)}{w_+ - w_-}, \quad B_{1-} = \frac{-(a_1w_- + b_1)(-b_1 + w_+b_2)}{w_+ - w_-},\\
A_{2+} &= \frac{(a_2w_+ + b_2)(-a_1 + w_-a_2)}{w_+ - w_-}, \quad A_{2-} = \frac{-(a_2w_- + b_2)(-a_1 + w_+a_2)}{w_+ - w_-}\\
\text{and} \qquad B_{2+} &= \frac{(a_2w_+ + b_2)(-b_1 + w_-b_2)}{w_+ - w_-}, \quad B_{2-} = \frac{-(a_2w_- + b_2)(-b_1 + w_+b_2)}{w_+ - w_-}.
\end{aligned}\right\} \tag{4.16}$$

Now all components of the Langevin equation (2.4), being the Markovian terms (4.5), the noise terms (4.12) and the memory integrands (4.15), are known. Thus we can write down the result of applying the MZ formalism to the discretized AMO system (4.1)

$$\left.\begin{aligned}
\partial_t T_1^0 &= -a_1NT_1^0 - b_1NT_2^0 - \alpha T_1^0\\
&\quad + N\,\mathrm{e}^{-\alpha t}\sum_{i=1}^{N-1}\Big((a_1w_+ + b_1)\,\mathrm{e}^{-l_+Nt}c_+^i + (a_1w_- + b_1)\,\mathrm{e}^{-l_-Nt}c_-^i\Big)\frac{t^{i-1}}{(i-1)!}\\
&\quad + \int_0^t N^2\frac{(t-s)^{N-2}}{(N-2)!}\,\mathrm{e}^{-\alpha(t-s)}\Big((l_+N)^{N-2}\,\mathrm{e}^{-l_+N(t-s)}\big(A_{1+}T_1^0(s) + B_{1+}T_2^0(s)\big)\\
&\quad + (l_-N)^{N-2}\,\mathrm{e}^{-l_-N(t-s)}\big(A_{1-}T_1^0(s) + B_{1-}T_2^0(s)\big)\Big)\mathrm{d}s,\\
\partial_t T_2^0 &= -a_2NT_1^0 - b_2NT_2^0 - \alpha T_2^0\\
&\quad + N\,\mathrm{e}^{-\alpha t}\sum_{i=1}^{N-1}\Big((a_2w_+ + b_2)\,\mathrm{e}^{-l_+Nt}c_+^i + (a_2w_- + b_2)\,\mathrm{e}^{-l_-Nt}c_-^i\Big)\frac{t^{i-1}}{(i-1)!}\\
&\quad + \int_0^t N^2\frac{(t-s)^{N-2}}{(N-2)!}\,\mathrm{e}^{-\alpha(t-s)}\Big((l_+N)^{N-2}\,\mathrm{e}^{-l_+N(t-s)}\big(A_{2+}T_1^0(s) + B_{2+}T_2^0(s)\big)\\
&\quad + (l_-N)^{N-2}\,\mathrm{e}^{-l_-N(t-s)}\big(A_{2-}T_1^0(s) + B_{2-}T_2^0(s)\big)\Big)\mathrm{d}s.
\end{aligned}\right\} \tag{4.17}$$

This system depends on the discretization or, more precisely, on the number of points N. Ideally, we would like to find the equations for the continuous model. The limiting behaviour as $N \to \infty$, or $1/N = \epsilon \to 0$, of the different terms is studied in the electronic supplementary material. The equations obtained after taking this limit can be written as

$$\left.\begin{aligned} \epsilon \frac{\mathrm{d}T_1}{\mathrm{d}t} &= -a_1 T_1(t) - b_1 T_2(t) + A_{1+}\tau_+ \mathrm{e}^{-\alpha\tau_+} T_1(t-\tau_+) + B_{1+}\tau_+ \mathrm{e}^{-\alpha\tau_+} T_2(t-\tau_+) \\ &\quad + A_{1-}\tau_- \mathrm{e}^{-\alpha\tau_-} T_1(t-\tau_-) + B_{1-}\tau_- \mathrm{e}^{-\alpha\tau_-} T_2(t-\tau_-) + \epsilon f_{\epsilon 1}(t) + \mathcal{O}(\epsilon^2) \\ \text{and} \quad \epsilon \frac{\mathrm{d}T_2}{\mathrm{d}t} &= -a_2 T_1(t) - b_2 T_2(t) + A_{2+}\tau_+ \mathrm{e}^{-\alpha\tau_+} T_1(t-\tau_+) + B_{2+}\tau_+ \mathrm{e}^{-\alpha\tau_+} T_2(t-\tau_+) \\ &\quad + A_{2-}\tau_- \mathrm{e}^{-\alpha\tau_-} T_1(t-\tau_-) + B_{2-}\tau_- \mathrm{e}^{-\alpha\tau_-} T_2(t-\tau_-) + \epsilon f_{\epsilon 2}(t) + \mathcal{O}(\epsilon^2), \end{aligned}\right\} \tag{4.18}$$

where

$$\left.\begin{aligned} f_{\epsilon 1}(t) &= -\alpha T_1(t) + A_{1+}\tau_+ \mathrm{e}^{-\alpha\tau_+} g_{\epsilon+}(T_1) + B_{1+}\tau_+ \mathrm{e}^{-\alpha\tau_+} g_{\epsilon+}(T_2) \\ &\quad + A_{1-}\tau_- \mathrm{e}^{-\alpha\tau_-} g_{\epsilon-}(T_1) + B_{1-}\tau_- \mathrm{e}^{-\alpha\tau_-} g_{\epsilon-}(T_2), \\ f_{\epsilon 2}(t) &= -\alpha T_2(t) + A_{2+}\tau_+ \mathrm{e}^{-\alpha\tau_+} g_{\epsilon+}(T_1) + B_{2+}\tau_+ \mathrm{e}^{-\alpha\tau_+} g_{\epsilon+}(T_2) \\ &\quad + A_{2-}\tau_- \mathrm{e}^{-\alpha\tau_-} g_{\epsilon-}(T_1) + B_{2-}\tau_- \mathrm{e}^{-\alpha\tau_-} g_{\epsilon-}(T_2), \end{aligned}\right\} \tag{4.19}$$

for

$$g_{\epsilon\pm}(T) = \frac{\tau_\pm^2}{2}\left(\left((l_\pm+\alpha)^2 - \frac{7}{6}l_\pm^2\right)T(t-\tau_\pm) + 2(l_\pm+\alpha)T'(t-\tau_\pm) + T''(t-\tau_\pm)\right), \tag{4.20}$$

with $\tau_\pm = 1/l_\pm$ and T' and T'' the derivatives of T. Note that we have dropped the superscript 0 in the notation, as the system found is valid at every location throughout the basin through a simple coordinate transformation. In (4.18), the first two terms (without delay) in the equations for $T_{1,2}$ are the Markovian terms, while the terms including a delay result from the memory term. In (4.19), the α-term comes from the Markovian part, while the terms including $g_{\epsilon\pm}$ can be attributed to the memory term. This is the final result of the application of the MZ formalism to the AMO model (3.4) as an expansion in terms of order ϵ. Letting $\epsilon \to 0$ a set of delay-difference equations is found, giving the exact reduced model of the AMO.

When applying the MZ formalism to the extended AMO model as derived in §3b, the leading-order terms change slightly. The $\mathrm{e}^{-\alpha\tau_\pm}$ terms change to $\mathrm{e}^{-(\alpha+l_\pm^1)\tau_\pm}$ with $l_\pm^1$ the additional first-order term of the eigenvalues of the orthogonal dynamics system for the extended AMO model. This leads to additional damping of the high-frequency modes as l_+^1 is positive, i.e. reducing the effect of the terms with a short delay time τ_+. On the other hand, l_-^1 is negative, weakening the damping of the low-frequency mode (and making it weakly unstable for $\alpha = 0$). This corresponds to the observed weakening of the high-frequency modes as discussed in §3b.

(d) Delay model derived via wave characteristics

The MZ formalism is in principle applicable also when the coefficients a_j and b_j are space dependent. However, in that case it may not be possible to derive explicit expressions for delays and coefficients in (4.18). For spatially constant coefficients a_j and b_j and equal damping α in all components, we may also derive the leading orders of (4.18) by integration along wave characteristics. This approach is similar to that taken in [2] and we refer to it as the MoC. The damped free-wave solutions of the two-layer system,

$$\left.\begin{aligned} \partial_t T_1 &= a_1 \partial_x T_1 + b_1 \partial_x T_2 - \alpha T_1 \\ \text{and} \quad \partial_t T_2 &= a_2 \partial_x T_1 + b_2 \partial_x T_2 - \alpha T_2, \end{aligned}\right\} \tag{4.21}$$

can be split into the decoupled equations

$$\partial_t \tilde{T}_\pm - l_\pm \partial_x \tilde{T}_\pm + \alpha \tilde{T}_\pm = 0, \tag{4.22}$$

Table 3. Parameters used in numerical computations of (4.28). Note that these are approximated from equation (4.23) using the values in table 2.

l_+	l_-	τ_+	τ_-
0.3527	0.0375	2.83	26.65

along the wave characteristics, where the characteristic speeds and delays

$$l_\pm = \frac{1}{2}\left[a_1 + b_2 \pm \sqrt{(a_1+b_2)^2 - 4a_1b_2 + 4a_2b_1}\right], \quad \tau_\pm = \frac{1}{l_\pm}, \tag{4.23}$$

are the same as for the MZ formalism in (4.8). The new variables $\tilde{T}_\pm$ are related back to the original variables through the transformation T_P,

$$\vec{T} = T_P \begin{bmatrix} \tilde{T}_+ \\ \tilde{T}_- \end{bmatrix}, \quad \text{where } T_P = \begin{bmatrix} \dfrac{a_1 - l_+}{a_2} & \dfrac{a_1 - l_-}{a_2} \\ 1 & 1 \end{bmatrix}, \; T_P^{-1} = \begin{bmatrix} \dfrac{-a_2}{l_+ - l_-} & \dfrac{a_1 - l_-}{l_+ - l_-} \\ \dfrac{a2}{l_+ - l_-} & \dfrac{l_+ - a_1}{l_+ - l_-} \end{bmatrix}. \tag{4.24}$$

The damped wave equations (4.22) have the general solutions

$$\tilde{T}_\pm(t,x) = \tilde{T}^0_\pm(t + x\tau_\pm)\mathrm{e}^{-\alpha x \tau_\pm}, \tag{4.25}$$

where the arbitrary profiles $\tilde{T}^0_\pm$ are constrained by the boundary conditions $\tilde{T}_\pm(t,0) = -\tilde{T}_\pm(t,1)$. These boundary conditions enforce the delay-difference equations for $\tilde{T}^0_\pm$,

$$\tilde{T}^0_\pm(t) = -\mathrm{e}^{-\alpha\tau_\pm}\tilde{T}^0_\pm(t - \tau_\pm), \tag{4.26}$$

after shifting t by $\tau_\pm$ and multiplying both sides by $\mathrm{e}^{-\alpha\tau_\pm}$ in the boundary conditions. Transforming $\tilde{T}^0(t)$ back using the transformation T_P^{-1} gives the coupled delay equations

$$\vec{T}(t) = \mathrm{e}^{-\alpha\tau_+}C_1\vec{T}(t - \tau_+) + \mathrm{e}^{-\alpha\tau_-}C_2\vec{T}(t - \tau_-) \tag{4.27}$$

(dropping the superscript 0 of $\tilde{T}$ for ease of notation) with

$$C_1 = \begin{bmatrix} \dfrac{l_- - a_1}{l_+ - l_-} & \dfrac{(l_+ - a_1)(l_- - a_1)}{a_2(l_+ - l_-)} \\ -\dfrac{a2}{l_+ - l_-} & -\dfrac{l_+ - a_1}{l_+ - l_-} \end{bmatrix} \quad \text{and} \quad C_2 = \begin{bmatrix} -\dfrac{l_+ - a_1}{l_+ - l_-} & -\dfrac{(l_+ - a_1)(l_- - a_1)}{a_2(l_+ - l_-)} \\ \dfrac{a_2}{l_+ - l_-} & \dfrac{l_+ - a_1}{l_+ - l_-} \end{bmatrix}.$$

The above is valid at every location in the basin according to the general solution form (4.25), as discussed in §4c. The MZ derived system in equation (4.18) for $\epsilon = 0$ can be rewritten to the above system.

System (4.27) is a delay-difference system. In order to explore solutions of the delay-difference system, we convert (4.27) to a system of delay differential equations (DDEs) by regularizing it with a small time derivative $\epsilon \mathrm{d}\vec{T}/\mathrm{d}t$,

$$\epsilon\frac{\mathrm{d}\vec{T}(t)}{\mathrm{d}t} = -\vec{T}(t) + \mathrm{e}^{-\alpha\tau_+}C_1\vec{T}(t - \tau_+) + \mathrm{e}^{-\alpha\tau_-}C_2\vec{T}(t - \tau_-), \tag{4.28}$$

with $\epsilon \ll 1$. The choice of ϵ is related to the discretization of the original PDE system (4.21) through $\epsilon = 1/N$, where N is the number of discretization steps using an 'upwind' scheme (discretizing in the direction of the wave). Table 3 shows the approximate resulting wave speeds and delays when using the parameter values in table 2 for our numerical solutions and spectral analysis, which are discussed in the next section.

5. Analysis of delay models

In this section, we analyse the solutions of the delay-difference models derived via the MZ formalism (4.18) and the MoC (4.28). We start with a discussion of the asymptotic spectrum and a spectral analysis of the MoC model (4.28). Next, we discuss the error terms as computed using the MZ formalism, followed by a comparison of the MZ delay model, the MoC delay model and the numerical PDE solution from which the MZ model is derived.

(a) Asymptotic spectrum of delay models

We observe that the delays occurring in the MoC system are of different magnitude: $\tau_+ \ll \tau_-$, where τ_+ is of order $O(1)$ in the time scale of (4.28). For hierarchical large delays, Yanchuk and co-workers [28,29] provide a simple approximation of the spectrum for (4.28), which captures the range of possible curvatures of the curves along which the eigenvalues shown in figure 6 align. Any eigenvalue λ of (4.28) satisfies

$$\det\left[-\epsilon\lambda I - I + C_1 \mathrm{e}^{-(\alpha+\lambda)\tau_+} + C_2 \mathrm{e}^{-(\alpha+\lambda)\tau_-}\right] = 0, \tag{5.1}$$

with $\epsilon \ll 1$, $\tau_+ = O(1)$ and $\tau_+ \ll \tau_-$. Hence, the term $\mathrm{e}^{-(\alpha+\lambda)\tau_-}$ is negligibly small unless $\alpha\tau_-$ and $\mathrm{Re}\,\lambda\tau_-$ are of order 1 or less. If we assume that this is the case, we may introduce $\alpha_- = \alpha/\tau_-$ (which is of order 1 or less) and look for eigenvalues λ of the form $\lambda = \gamma/\tau_+ + \mathrm{i}\omega/\epsilon$ (called the pseudo-continuous spectrum in [28]). Then $(\gamma + \alpha_-)\tau_+/\tau_-$ and $\epsilon\gamma/\tau_-$ are small. Dropping these terms and introducing the phases $\phi_\pm = \omega\tau_\pm/\epsilon$ and $z = \mathrm{e}^{-(\gamma+\alpha_-)+\mathrm{i}\phi_-}$ simplifies (5.1) to

$$\det\left[-\mathrm{i}\omega I - I + C_1 \mathrm{e}^{\mathrm{i}\phi_+} + C_2 z\right] = 0. \tag{5.2}$$

Equation (5.2) is in our case a quadratic equation in the complex number z, giving two roots, each depending on ω and ϕ_+, which one may express as $z_\pm(\omega, \phi_+)$. From this root pair, one may derive the damping depending on the frequency, $\gamma_\pm(\omega, \phi_+) = -\alpha_- + \log z_\pm(\omega, \phi_+)$, and, in the original scaling for eigenvalue λ,

$$\mathrm{Re}\,\lambda = -\alpha + \tau_+ \log z_\pm(\epsilon\,\mathrm{Im}\,\lambda, \phi_+).$$

This relation determines the curves along which the eigenvalues align for positive small ϵ and $\tau_+ \ll \tau_-$. The phase ϕ_+ is treated here as an independent parameter. It is very sensitive with respect to small changes of τ_+ (since $\phi_+ = \omega\tau_+/\epsilon$) such that the location of the eigenvalue curves will vary strongly depending on τ_+ or ϵ within the range given by $\phi_+ \in [0, 2\pi]$. Ruschel & Yanchuk's [29] analysis shows in general that for hierarchically large delays the spectrum 'fills an area' of the complex plane under small parameter variations.

(b) Spectral analysis of trajectories

For the spectral analysis of the MoC delay model (4.28) (with $\alpha = 0$), we compute the trajectories of T_1 and T_2. To compute the history needed for the difference equation, the PDE system (4.21) is solved numerically for an initial profile of the basin using an upwind discretization scheme for τ_- years. We take a Gaussian initial distribution profile (same as figure 4*a*). The DDE system (4.28) is then evolved for a further 200 time steps. Figure 7 shows the results.

A spectral analysis is performed on the resulting trajectories to identify the most prominent oscillation periods. A dominant signal of a $2\tau_-$ year cycle is obtained, along with a smaller signal for a $2\tau_+$ year cycle. These two most prominent signals correspond to period doubling of the two delay values which arises naturally from the boundary conditions. There is a smaller peak corresponding to a cycle of approximately $\frac{2}{3}\tau_-$ years. The signals corresponding to $2\tau_-$ (53.07) and $\frac{2}{3}\tau_-$ (17.77) year cycles align with the literature regarding possible cycle lengths of the AMO [7,9]. The signal corresponding to the $2\tau_+$ year cycle is much less pronounced in the surface temperature than in the subsurface temperature.

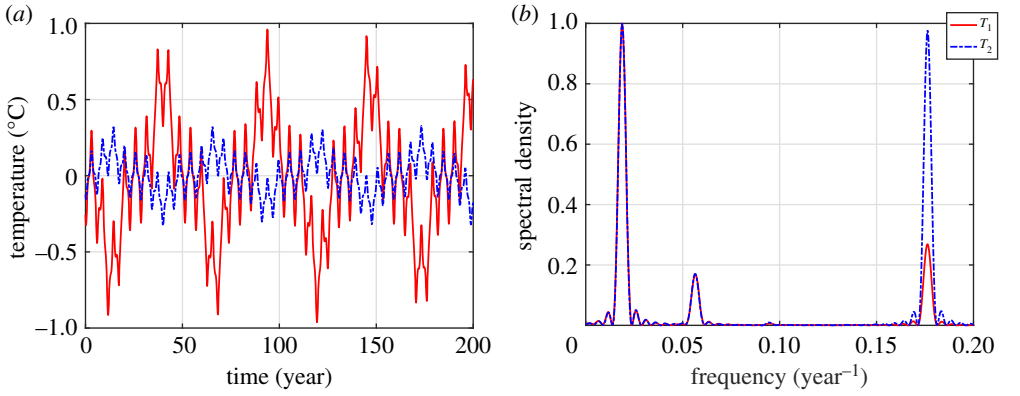

Figure 7. Numerical results for (4.28) with parameters from table 3 and $\alpha = 0$. (*a*) Trajectory for 200 years. (*b*) Power spectral density. (Online version in colour.)

Table 4. Sensitivity analysis on basin length (W, km) and effect on dominant cycles (years) for $\alpha = 0$.

latitude	W	$2\tau_-$	$\frac{2}{3}\tau_-$	$2\tau_+$
10° N	6540	87.15	29.05	9.27
20° N	6240	83.15	27.72	8.85
30° N	5760	76.75	25.58	8.17
40° N	5100	67.96	22.65	7.23
50° N	4260	56.77	18.92	6.04
60° N	3360	44.77	14.92	4.76
70° N	2280	30.38	10.13	3.23

The length of the cycles will naturally be dependent upon the basin size chosen. Here, we use a zonal basin size of 4000 km, which corresponds to the width of the basin at 52° N. The basin was defined in [17] to have latitudinal boundaries of 10° N and 70° N. The zonal basin width for a longitudinal extent of 60° varies between these latitudes. We have, therefore, performed a sensitivity analysis on the basin width for a selection of latitudes and computed the resulting dominant cycle lengths. The results of this are listed in table 4. The range of cycle lengths, particularly those associated with $2\tau_-$ and $\frac{2}{3}\tau_-$, generally agree with the range of those identified in observational products. Measurements of SST have shown oscillations with a period between 50 and 70 years [30,31], while an analysis of subsurface temperature identifies a 20–30 year oscillation [32]. The first period of 50–70 years corresponds to $2\tau_-$, while the shorter period of 20–30 years roughly matches $\frac{2}{3}\tau_-$, with the best correspondence found for latitudes around 40° N.

(c) Comparison of delay models

We start this section with an evaluation of the theoretical error terms $f_{\epsilon,i}$ for $i = 1, 2$ (equation (4.19)) as computed via the MZ formalism. An example of the evolution of these terms has been plotted in figure 8*a*. Also shown is the decrease in their maximum amplitude with increasing N (decreasing ϵ), which corresponds to the effect expected from increasing the number of steps in a discretized PDE. Thus the theoretical error of the delay system derived using the MZ formalism (4.18) indicates that the delay model exhibits an error similar to that of the discretized PDE. In figure 8*b* the spectral density of $f_{\epsilon i}$ for $i = 1, 2$ is shown. We find a peak at a frequency of 0.53 year^{-1}, which emerges owing to second derivatives in the computation of $f_{\epsilon i}$. The small

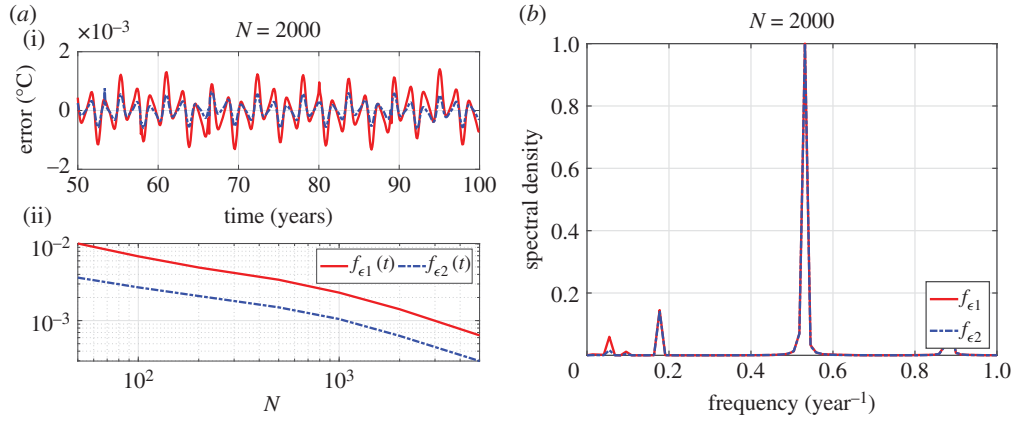

Figure 8. The error terms $f_{\epsilon 1}, f_{\epsilon 2}$ as computed using the MZ formalism with parameters from table 3 and $\alpha = 0$. (*a*) The change of amplitude of the terms with N is shown together with an example of the error terms for $N = 2000$. (*b*) The spectrum of $f_{\epsilon 1}$ and $f_{\epsilon 2}$. (Online version in colour.)

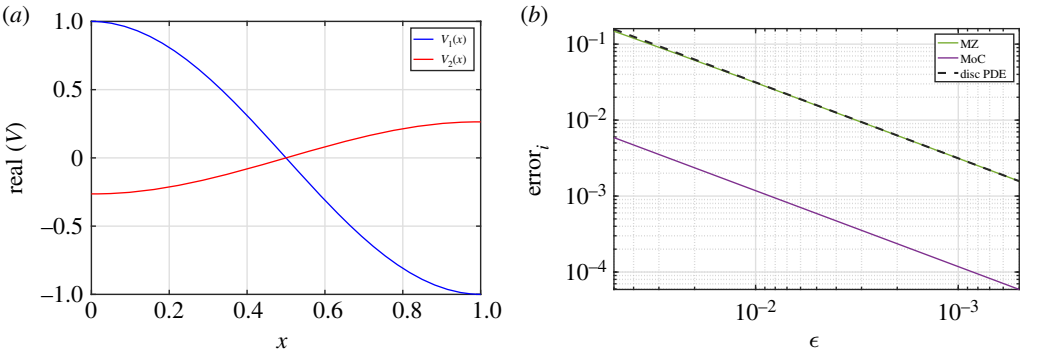

Figure 9. (*a*) The real part of the eigenfunctions of the PDE and (*b*) the errors of the discretized PDE (plotted for $\epsilon = \frac{1}{N}$), MoC and MZ model as calculated using the eigenfunctions (with $\alpha = 0$). (Online version in colour.)

low-frequency peaks correspond to those of the exact delay model, as shown in figure 7*b*, as there is a delayed contribution from the temperature itself (and its first derivative) to the error term as well.

Next, we compare the performance of the two DDE models derived via the MZ projection (§4a–c) and the MoC (§4d) with the exact and discretized PDE models. We do this through the calculation of the eigenfunctions of the respective models. Figure 9*a* shows the real part of the eigenfunctions for each component of the exact PDE calculated using the Chebfun open-source software [33]. We also compute the eigenfunctions for each approximation to the exact PDE: discretized PDE, delay via MoC, and delay via MZ. We scale all the eigenfunctions such that $V_1(x = 0) = 1$. In order to compare the relative approximations, we calculate the error with respect to the eigenfunctions satisfying the PDE boundary conditions (3.2)

$$\text{error}_i := |V_1^i(x = 0) + V_1^i(x = 1)| \quad \text{for } i \in \{\text{disc PDE, MoC, MZ}\}. \tag{5.3}$$

As the approximate systems approach the exact PDE, the eigenfunctions of the respective models are expected to converge and therefore satisfy the PDE boundary conditions. We then would expect (5.3) to approach zero as N (ϵ) is increased (decreased) if the models are good approximations of the exact PDE. We calculate (5.3) for a range of N and ϵ values and plot the respective errors in figure 9*b*. It can be seen that decreasing the ϵ term in the delay equations has

the same effect on the approximation to the exact PDE as increasing N in the discretization. In other words, the error introduced through the ϵ term in the 'smoothing' approximation of delay-difference equations is proportional to the error introduced by discretization methods of wave equation PDEs ($\epsilon \propto 1/N$).

6. Summary, discussion and conclusion

A delay model for the AMO has been derived from a three-layer model by Sévellec & Huck [17] using the MZ formalism. This formalism gives a rewriting of a system of ODEs [3] which contains a Markovian, a noise and a memory term. The advantage of this delay model, over, for example, mode decomposition, is that it precisely shows the propagating wave nature of the AMO, through the (inverse) travel times $l_{\pm}$, hence providing more support for the thermal Rossby wave mechanism proposed in [16]. In a similar way to the ENSO delayed oscillator model [4,34], this model can also be used to study the effects of background state, non-stationary forcing, noise and possibly state-dependent delay versions on the behaviour of the AMO [35,36].

The derived model for the AMO is a first-order delay-difference model, in contrast to the delay differential model for ENSO [2]. This means that the current state is fully determined by past states. This type of model can exhibit an increasing switching frequency between states [37], making it physically unrealistic. Hence, an $\epsilon \frac{\mathrm{d}}{\mathrm{d}t}$-term was added to prevent this behaviour and allow for better numerical treatment. We were able to derive an error term for this approximation using the MZ formalism, and relate this error to the upwind discretization scheme used in solving the original PDE model. For the non-damped version of the AMO model ($\alpha = 0$), the MZ formalism is not strictly necessary for deriving a delay model, although it is more general and can be extended to other types of models. The MoC yields the same delay-difference equation, as shown in §5d. We showed that the way in which the smoothing approximation $\epsilon \frac{\mathrm{d}}{\mathrm{d}t}$-term is added affects the size of the error of the delay model. Furthermore, the error introduced through the smoothing $\epsilon \frac{\mathrm{d}}{\mathrm{d}t}$-term is proportional to that introduced by discretization methods, as discussed in §5c.

The PDE model of the AMO by Sévellec & Huck [17], the starting point for deriving the delay model, does not contain a background overturning circulation. This results in a high-frequency model oscillation which is undesired to study the AMO. As discussed in §3b, adding the meridional overturning circulation to the background state of the model results in a damping of this high-frequency oscillation. This also becomes clear when studying the delay model corresponding to this extended AMO model, which has been derived in the electronic supplementary material. It shows a weakening of the delayed effect of the high-frequency mode (short delay time), while the low-frequency mode (long delay time) is enhanced by the extended background state.

The method of deriving delay equations as applied to a PDE model of the AMO (and also to a PDE model of ENSO [2]) can be generalized. It is expected that any diagonalizable linear system of wave equations can be rewritten in the form of a delay-difference system, given sufficient coupling that allows for the transfer of a signal between either different variables or boundaries. Integration along characteristics would yield the dominant terms, but the MZ formalism additionally gives error terms to a smoothing approximation for solving the delay-difference system. The necessity of the diagonalizability remains to be investigated. For non-diagonalizable systems, it is not yet clear whether a similar result would hold as the computations become more involved.

For nonlinear models the method applied here to the AMO model has to be generalized. Although the MZ formalism is general and does not rely on the linearity of the system, the difficulty lies in solving the orthogonal dynamics equation, as noted extensively in the literature [3,21,23]. For linear models, the pseudo-orthogonal dynamics approximation can be used to arrive at the final result [38]. For nonlinear models, this approximation cannot be used without first showing its accuracy. In [2] it was shown to result in a significant error for the nonlinear ENSO model studied. A better approximation for nonlinear models first needs to be proposed before

the method described here can be accurately generalized. This step is necessary for a reliable and accurate application of the MZ formalism to nonlinear models of climate phenomena.

Many PDE models used to describe climate phenomena contain some type of wave dynamics. We have shown in this study that projecting a system of wave equations onto one location yields a delay model. This would imply that more climate variability phenomena could be described by a delay equation when there is a physical mechanism that suggests memory effects. Once better methods of approximation of the orthogonal dynamics are available, it may be possible to derive accurate nonlinear delay models of climate phenomena, thus clarifying dynamical mechanisms and allowing for further analysis.

Data accessibility. The codes supporting this article have been uploaded as part of the electronic supplementary material.

Authors' contributions. S.K.J.F., C.Q. and H.A.D. designed the study. The work was carried out mainly by S.K.J.F. and C.Q. J.S. designed the analysis and comparison of the delay models in §5. All authors contributed to the work, discussed the results and read and approved the manuscript.

Competing interests. We declare we have no competing interests.

Funding. This work was supported by funding from the European Union Horizon 2020 research and innovation programme for the ITN CRITICS under grant agreement no. 643073 (C.Q., J.S. and H.A.D.). S.K.J.F. was supported by the Centre for Doctoral Training in Mathematics of Planet Earth, UK EPSRC funded (grant no. EP/L016613/1) and J.S. by EPSRC grants nos. EP/N023544/1 and EP/N014391/1.

Acknowledgements. We thank Bruno Deremble and the anonymous reviewer for their constructive comments. S.K.J.F. thanks the University of Exeter for hosting her for five months in 2018.

References

1. Keane A, Krauskopf B, Postlethwaite CM. 2017 Climate models with delay differential equations. *Chaos* **27**, 114309. (doi:10.1063/1.5006923)
2. Falkena SKJ, Quinn C, Sieber J, Frank J, Dijkstra HA. 2019 Derivation of delay equation climate models using the Mori-Zwanzig formalism. *Proc. R. Soc. A* **475**, 20190075. (doi:10.1098/rspa.2019.0075)
3. Chorin AJ, Hald OH, Kupferman R. Optimal prediction with memory. *Physica D* **166**, 239–257. (doi:10.1016/S0167-2789(02)00446-3)
4. Suarez MJ, Schopf PS. 1988 A delayed action oscillator for ENSO. *J. Atmos. Sci.* **45**, 3283–3287. (doi:10.1175/1520-0469(1988)045<3283:ADAOFE>2.0.CO;2)
5. Enfield DB, Mestas-Nunez AM, Trimble PJ. 2001 The Atlantic Multidecadal Oscillation and its relationship to rainfall and river flows in the continental U.S. *Geophys. Res. Lett.* **28**, 2077–2080. (doi:10.1029/2000GL012745)
6. Deser C, Alexander MA, Xie S-P, Phillips AS. 2010 Sea surface temperature variability: patterns and mechanisms. *Annu. Rev. Mar. Sci.* **2**, 115–143. (doi:10.1146/annurev-marine-120408-151453)
7. Chylek P, Folland CK, Dijkstra HA, Lesins G, Dubey MK. 2011 Ice-core data evidence for a prominent near 20 year time-scale of the Atlantic Multidecadal Oscillation. *Geophys. Res. Lett.* **38**, L13704. (doi:10.1029/2011GL047501)
8. Cheung AH, Mann ME, Steinman BA, Frankcombe LM, England MH, Miller SK. 2017 Comparison of low-frequency internal climate variability in CMIP5 models and observations. *J. Clim.* **30**, 4763–4776. (doi:10.1175/JCLI-D-16-0712.1)
9. Delworth TL, Mann ME. 2000 Observed and simulated multidecadal variability in the Northern Hemisphere. *Clim. Dyn.* **16**, 661–676. (doi:10.1007/s003820000075)
10. Frankcombe LM, von der Heydt A, Dijkstra HA. 2010 North Atlantic multidecadal climate variability: an investigation of dominant time scales and processes. *J. Clim.* **23**, 3626–3638. (doi:10.1175/2010JCLI3471.1)
11. Han Z, Luo F, Li S, Gao Y, Furevik T, Svendsen L. 2016 Simulation by CMIP5 models of the Atlantic Multidecadal Oscillation and its climate impacts. *Adv. Atmos. Sci.* **33**, 1329–1342. (doi:10.1007/s00376-016-5270-4)
12. Dijkstra HA. 2005 *Nonlinear physical oceanography*, vol. 28, 2nd revised edn. New York, NY: Springer.
13. Dijkstra HA. 2008 *Dynamical oceanography*. New York, NY: Springer.

14. Srokosz M, Baringer M, Bryden H, Cunningham S, Delworth T, Lozier S, Marotzke J, Sutton R. 2012 Past, present, and future changes in the Atlantic meridional overturning circulation. *Bull. Am. Meteorol. Soc.* **93**, 1663–1676. (doi:10.1175/BAMS-D-11-00151.1)
15. Verdière C de, Huck T. 1999 Baroclinic instability: an oceanic wavemaker for interdecadal variability. *J. Phys. Oceanogr.* **29**, 893–910. (doi:10.1175/1520-0485(1999)029<0893:BIAOWF>2.0.CO;2)
16. te Raa LA, Dijkstra HA. 2002 Instability of the thermohaline ocean circulation on interdecadal timescales. *J. Phys. Oceanogr.* **32**, 138–160. (doi:10.1175/1520-0485(2002)032<0138:IOTTOC>2.0.CO;2)
17. Sévellec F, Huck T. 2015 Theoretical investigation of the Atlantic Multidecadal Oscillation. *J. Phys. Oceanogr.* **45**, 2189–2208. (doi:10.1175/JPO-D-14-0094.1)
18. Mori H. 1965 Transport, collective motion and Brownian motion. *Prog. Theor. Phys.* **33**, 423–455. (doi:10.1143/PTP.33.423)
19. Zwanzig R. 1973 Nonlinear generalized Langevin equations. *J. Stat. Phys.* **9**, 215–220. (doi:10.1007/BF01008729)
20. Chorin AJ, Kupferman R, Levy D. 2000 Optimal prediction for Hamiltonian partial differential equations. *J. Comput. Phys.* **162**, 267–297. (doi:10.1006/jcph.2000.6536)
21. Darve E, Solomon J, Kia A. 2009 Computing generalized Langevin equations and generalized Fokker-Planck equations. *Proc. Natl Acad. Sci. USA* **106**, 10 884–10 889. (doi:10.1073/pnas.0902633106)
22. Morriss GP, Evans DJ. 2013 *Statistical mechanics of nonequilibrium liquids*. Canberra, Australia: ANU Press.
23. Zhu Y, Venturi D. 2018 Faber approximation of the Mori–Zwanzig equation. *J. Comput. Phys.* **372**, 694–718. (doi:10.1016/j.jcp.2018.06.047)
24. Dijkstra HA. 2006 Interaction of SST modes in the North Atlantic Ocean. *J. Phys. Oceanogr.* **36**, 286–299. (doi:10.1175/JPO2851.1)
25. Broer HW, Dijkstra HA, Simó C, Sterk AE, Vitolo R. 2011 The dynamics of a low-order model for the Atlantic multidecadal oscillation. *Discrete Continuous Dyn. Syst. Ser. B* **16**, 73–107. (doi:10.3934/dcdsb.2011.16.73)
26. Cushman-Roisin B, Beckers J. 2011 *Introduction to geophysical fluid dynamics*, vol. 101. New York, NY: Academic Press.
27. Zill DG, Cullen MR. 1997 *Differential equations with boundary value problems*, 7th edn. Belmont, CA: Brooks/Cole Cengage Learning.
28. Lichtner M, Wolfrum M, Yanchuk S. 2011 The spectrum of delay differential equations with large delay. *SIAM J. Math. Anal.* **43**, 788–802. (doi:10.1137/090766796)
29. Ruschel S, Yanchuk S. 2021 The spectrum of delay differential equations with multiple hierarchical large delays. *Discrete Continuous Dyn. Syst. S* **14**, 151–175.
30. Kushnir Y. 1994 Interdecadal variations in North Atlantic sea surface temperature and associated atmospheric conditions. *J. Clim.* **7**, 141–157. (doi:10.1175/1520-0442(1994)007<0141:IVINAS>2.0.CO;2)
31. Schlesinger ME, Ramankutty N. 1994 An oscillation in the global climate system of period 65–70 years. *Nature* **367**, 723–726. (doi:10.1038/367723a0)
32. Frankcombe LM, Dijkstra HA, Von der Heydt A. 2008 Sub-surface signatures of the Atlantic Multidecadal Oscillation. *Geophys. Res. Lett.* **35**, L19602. (doi:10.1029/2008GL034989)
33. Driscoll TA, Hale N, Trefethen LN. 2014 *Chebfun guide*. Oxford, UK: Pafnuty Publications.
34. Battisti DS, Hirst AC. 1989 Interannual variability in a tropical atmosphere-ocean model: influence of the basic state, ocean geometry and nonlinearity. *J. Atmos. Sci.* **46**, 1687–1712. (doi:10.1175/1520-0469(1989)046<1687:IVIATA>2.0.CO;2)
35. Keane A, Krauskopf B, Dijkstra HA. 2019 The effect of state dependence in a delay differential equation model for the El Niño Southern Oscillation. *Phil. Trans. R. Soc. A* **377**, 2153. (doi:10.1098/rsta.2018.0121)
36. Tziperman E, Stone L, Cane MA, Jarosh H. 1994 El Niño chaos: overlapping of resonances between the seasonal cycle and the Pacific Ocean-atmosphere oscillator. *Science* **264**, 72–74. (doi:10.1126/science.264.5155.72)
37. Ghil M, Zaliapin I, Coluzzi B. 2008 Boolean delay equations: a simple way of looking at complex systems. *Physica D* **237**, 2967–2986. (doi:10.1016/j.physd.2008.07.006)
38. Gouasmi A, Parish EJ, Duraisamy K. 2017 *A priori* estimation of memory effects in reduced-order models of nonlinear systems using the Mori–Zwanzig formalism. *Proc. R. Soc. A* **473**, 20170385. (doi:10.1098/rspa.2017.0385)